Surface-Directed Phase Separation of Conjugated Polymer Blends for Efficient Light-Emitting Diodes

ARTICLE *in* ADVANCED FUNCTIONAL MATERIALS · OCTOBER 2008

Impact Factor: 11.81 · DOI: 10.1002/adfm.200800287

5 AUTHORS, INCLUDING:

Zijian Zheng
The Hong Kong Polytechnic University
67 PUBLICATIONS **1,738** CITATIONS

SEE PROFILE

Wilhelm Huck
Radboud University Nijmegen
250 PUBLICATIONS **13,341** CITATIONS

SEE PROFILE

ADVANCED FUNCTIONAL MATERIALS

DOI: 10.1002/adfm.200800287

Surface-Directed Phase Separation of Conjugated Polymer Blends for Efficient Light-Emitting Diodes**

By *Keng-Hoong Yim, Zijian Zheng, Richard H. Friend, Wilhelm T. S. Huck,** and *Ji-Seon Kim**

The ability to control organic-organic interfaces in conjugated polymer blends is critical for further device improvement. Here, we control the phase separation in blends of poly(9,9-di-*n*-octylfluorene-*alt*-benzothiadiazole) (F8BT) and poly(9,9-di-*n*-octylfluorene-*alt*-(1,4-phenylene-((4-*sec*-butylphenyl)imino)-1,4-phenylene) (TFB) via chemical modification of the substrate by microcontact printing of octenyltrichlorosilane molecules. The lateral phase-separated structures in the blend film closely replicate the underlying micrometer-scale chemical pattern. We found nanometer-scale vertical segregation of the polymers within both lateral domains, with regions closer to the substrate being substantially pure phases of either polymer. Such phase separation has important implications for the performance of light-emitting diodes fabricated using these patterned blend films. In the absence of a continuous TFB wetting layer at the substrate interface, as typically formed in spin-coated blend films, charge carrier injection is confined in the well-defined TFB-rich domains. This confinement leads to high electroluminescence efficiency, whereas the overall reduction in the roughness of the patterned blend film results in slower decay of device efficiency at high voltages. In addition, the amount of surface out-coupling of light in the forward direction observed in these blend devices is found to be strongly correlated to the distribution of periodicity of the phase-separated structures in the active layer.

1. Introduction

Modern day organic semiconductor devices often consist of two, if not more active materials. The understanding of the electronic properties of these organic-organic semiconductor interfaces and control over their thin film morphologies, is of critical importance for further device optimization, as excitons could either be stabilized or destabilized at interfaces, producing efficient light-emitting diodes (LEDs) and photovoltaic cells, respectively.[1–3] For example, the band-edge offsets between the valence and conduction bands of dissimilar organic semiconductors at heterojunctions strongly influence the device characteristics.[4–6]

For solution-processed conjugated polymers, blending two or more polymers from a common solvent is a widely used strategy to combine their optoelectronic functionalities in the solid state, allowing a various range of tunability and processability.[7] The use of conjugated polymer blends has indeed been very successful in improving device efficiency.[8,9] For example, LEDs fabricated with poly(9,9-di-*n*-octylfluorene-*alt*-benzothiadiazole) (F8BT) blended with poly(9,9-di-*n*-octylfluorene-*alt*-(1,4-phenylene-((4-*sec*-butylphenyl)imino)-1,4-phenylene) (TFB) as the emissive layer show a significantly improved device performance, such as higher electroluminescence efficiencies (above $18\,\mathrm{Lm\,W^{-1}}$) and excellent stability under prolonged operation (more than 5000 h at $100\,\mathrm{cd\,m^{-2}}$).[4,10]

When polymer thin films are formed by spin-coating from blend solutions, phase separation typically occurs.[11] The interpenetrating network of the phase-separated blend provides distributed heterojunctions.[12,13] Such vertically and/or laterally phase-separated structures have important implications on fundamental optoelectronic processes including transport of charge carriers and recombination/dissociation of excitons, and surface out-coupling of light emission created inside the active layer.[14] For instance, ~100 nm-thick F8BT:TFB blend films spun from *xylene* solution typically show micrometer-scale lateral phase separation with very rough surface topography (~40–50 nm), along with nanoscale vertical phase segregation that produces a continuous TFB wetting layer and discontinuous TFB capping layer.[12] While such morphology of the blend film produces high initial electroluminescence (EL) efficiency due to confined charge carrier recombination at the polymer-polymer interfaces, the lower-lying domains provide pathways for leakage

[*] Prof. W. T. S. Huck, Z. Zheng
Melville Laboratory for Polymer Synthesis, University of Cambridge
Lensfield Road, Cambridge CB2 1EW (UK)
E-mail: wtsh2@cam.ac.uk
Prof. W. T. S. Huck, Z. Zheng
The Nanoscience Centre, University of Cambridge
J. J. Thomson Avenue, Cambridge CB3 0FF (UK)
Dr. J.-S. Kim, K.-H. Yim, Prof. R. H. Friend
Cavendish Laboratory, University of Cambridge
J. J. Thomson Avenue, Cambridge CB3 0HE (UK)
E-mail: jkim1@imperial.ac.uk
Dr. J.-S. Kim
Blackett Laboratory, Imperial College London, Prince Consort Road, London SW7 2AZ, UK
E-mail: jkim1@imperial.ac.uk

[**] The authors thank Cambridge Display Technology (CDT) Ltd. for the F8BT and TFB materials and financial support (K.-H. Y., Z. Z.), EPSRC for fund, Dorothy Hodgkin Postgraduate Studentship (Z. Z.) and Advanced Research Fellowship (J.-S. K.).

current at high voltages, thereby reducing the EL efficiency rapidly.[12,15]

Despite the successful use of conjugated polymer blends for various device applications, challenges ahead include precise control of the distribution of the heterojunction sites down to molecular level, to form ''ideal'' device architectures. Recent work on blend thin film morphology has shown that device efficiency can be greatly altered by changing the scale and direction of such phase separation.[8,15–17] For instance, surface-directed phase separation of poly(9,9′-dioctylfluorene) (PFO):F8BT blend has previously been exploited to fabricate LEDs having self-organized, two-dimensional (2D) photonic structures with nanoscale topography within the emissive layer. The patterned blend device showed improved device performance, achieving a maximum of ~1% external quantum efficiency (EQE) at ~40 mA cm^{-2} (~3.6 V), as a result of efficient out-coupling of light in the forward direction.[18,19]

In this paper, we show the control of the phase separation in F8BT:TFB blends to achieve a more desirable thin film morphology and thus more efficient LEDs by introducing a similar micrometer-scale chemical surface pattern to guide the phase-separation and by choosing appropriate polymer molecular weights and blend ratio. In addition, we present the detailed structure analysis of phase-separated blend thin films to explain the improved device performance. Phase separation in polymer blends is strongly dependent upon the surface energy of the substrate,[11,20,21] as well as solvent evaporation rate and other processing parameters. We use microcontact printing (μCP)[22,23] to create chemically patterned surfaces with periodic hydrophilic and hydrophobic areas. Upon spin-coating the blend solution, the less polar, low surface energy component of the blend will preferentially migrate away from regions of higher surface energy.[20] With appropriate choice of polymer molecular weights[24] and blend ratio,[25] it is possible to induce periodic phase-separated structures in the polymer blend film that replicate the underlying chemical pattern, provided the periodicity of the substrate pattern is comparable to the natural length scale for phase separation under the conditions used.

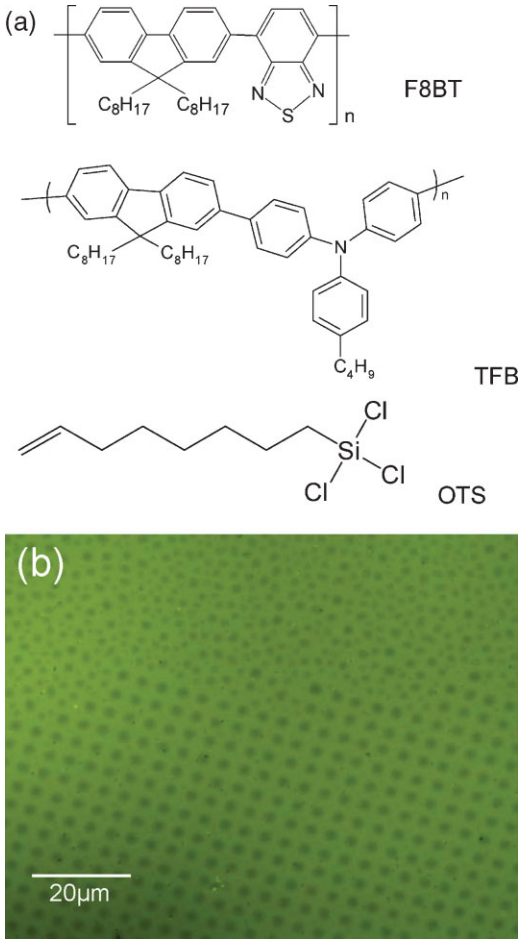

Figure 1. a) Chemical structures of F8BT, TFB and OTS materials. b) PL image of ~300 nm-thick patterned F8BT:TFB blend film (4:1 weight ratio) under blue excitation (2.85 eV). The bright regions in the PL image correspond to F8BT-rich phases while the dark regions correspond to TFB-rich phases. Note the contrast between the areas with and without the 2D pattern.

2. Results

The chemical structures of F8BT and TFB materials are shown in Figure 1a. In order to incorporate the polymer blend into working devices, the F8BT:TFB blend was deposited on poly(styrene sulphonate)-doped poly(3,4-ethylene dioxythiophene) (PEDOT:PSS), a hole-injection layer commonly used in organic devices. The hydrophilic PEDOT:PSS surface was chemically patterned by μCP of a self-assembled monolayer (SAM) of octenyltrichlorosilane (OTS, Fig. 1a), forming a 2D pattern of 2-μm-wide dots with a periodicity of 4 μm. A blend of F8BT:TFB was briefly spin-coated from *p*-xylene solution onto the OTS-patterned substrate and then left to dry slowly under saturated solvent atmosphere. Figure 1b shows the photoluminescence (PL) image of ~300 nm-thick F8BT:TFB blend film (4:1 by weight, $M_n = 62$ and 66 kg mol^{-1}, respectively) deposited on a chemically patterned PEDOT:PSS layer, under blue excitation (2.85 eV). Such selective excitation of F8BT allows quick qualitative identification of the phase-separated domains, as it results in green luminescence from F8BT while TFB remains dark.

The phase separation of the blend film closely replicates the substrate pattern over large area (several cm^2). Self-organization of polymers in the blend film is achieved in the presence of alternating hydrophilic PEDOT:PSS and hydrophobic OTS surfaces. F8BT is more polar due to the presence of benzothiadiazole (BT) groups on the polymer backbone and is preferentially deposited on the hydrophilic oxygen-plasma treated PEDOT:PSS as expected, while TFB accumulates on the hydrophobic areas defined by SAM. The patterned phase-separated structures are of comparable length scale to those formed under the same conditions on unpatterned surfaces

ADVANCED FUNCTIONAL MATERIALS

(top part of the PL image). We note that the quality of the pattern replication in the blend film is highly sensitive to the choice of polymer blend ratio and molecular weight combination of both polymers. A F8BT:TFB weight ratio of 4:1 was found to produce phase separation that replicates the pattern most closely, in good agreement with the surface coverage percentage by the OTS (~20%). High molecular weight ($M_n > 100\,kg\,mol^{-1}$) polymers lack chain mobility to fully separate from one another, while the natural length scale for phase separation in blends with low molecular weight ($M_n < 10\,kg\,mol^{-1}$) polymers (nanometer scale) is much smaller than the micrometer-scale pattern used here.[15]

The corresponding tapping mode atomic force microscope (AFM) image of the patterned F8BT:TFB blend film is shown in Figure 2a. As indicated by the surface line scan, the height difference between the lower-lying TFB (or TFB-rich) domains and the higher-lying F8BT (or F8BT-rich) domains is ~30 nm, while the blend film thickness is ~300 nm. We note that in contrast to a similar patterned blend film of PFO:F8BT,[18,19] we do not observe nanoscale "ripple" structures along the phase-separated domain boundaries in this patterned F8BT:TFB blend film, which might be attributed to higher solubility of TFB in *p*-xylene than F8BT (as oppose to lower solubility of PFO in *p*-xylene than F8BT).[18] The mechanism behind the formation of the "ripple" structures is not well understood, but it could be related to surface energy differences at the boundaries of the two polymer solutions, which lead to concave/convex surfaces as solvent continues to evaporate.[18,19,26] This subtle difference in the blend film topography might have significant impact on the device performance, as will be discussed later.

F8BT:TFB blend films (1:1 by weight, ~80–100 nm-thick) spin-coated on homogeneous surfaces shown in Figure 2b typically exhibit micrometer-scale lateral phase separation where the height difference between the phase-separated structures is usually ~40–50 nm.[12,15] This difference implies substantial reduction in the overall surface roughness of the patterned blend film while retaining micrometer-scale lateral phase segregation. On the other hand, F8BT:TFB blend films with 4:1 by weight composition (~80–100 nm-thick) shown in Figure 2c reveal smaller phase-separated structures (sub-micrometer length scale) with average roughness of ~10–20 nm. We predict that the blend composition of 4:1 will likely show nucleation driven behavior during the phase separation process, as opposed to spinodal decomposition observed in 1:1 blend, which typically leads to coarse features developed on relatively large length scales with rough surfaces.[12]

We fabricated LEDs with the patterned blend films and compared the devices to those with F8BT:TFB blend films of different blend compositions spin-coated on non-patterned substrates. The electroluminescence (EL) efficiency ($Cd\,A^{-1}$ and $Lm\,W^{-1}$)–voltage characteristics of these LEDs (area of each pixel is ~4.5 mm^2) are plotted in Figure 3a and b. All the devices exhibit sharp turn-on in both current and luminance at ~2 V (vs. ~2.5 V for PFO:F8BT blend devices).[18,19] In general, F8BT:TFB produces significantly more efficient blend devices

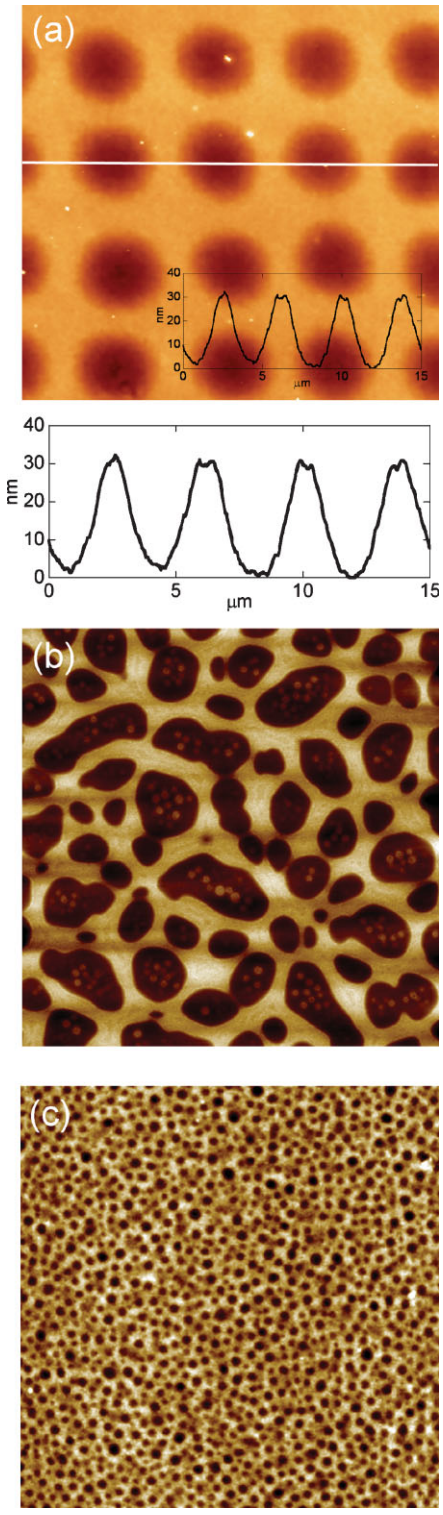

Figure 2. a) AFM image (15 μm × 15 μm, on 70 nm height scale) of the patterned F8BT:TFB blend film. Surface line scan (below) indicates that the height difference between the higher-lying F8BT-rich and lower-lying TFB-rich phases is ~30 nm. AFM images (20 μm × 20 μm) of ~80-nm-thick F8BT:TFB blend films spin-coated on non-patterned substrates, with compositions of b) 1:1 (on 70 nm height scale) and c) 4:1 by weight (on 20 nm height scale). In both blend films the lower-lying domains are TFB-rich phases.

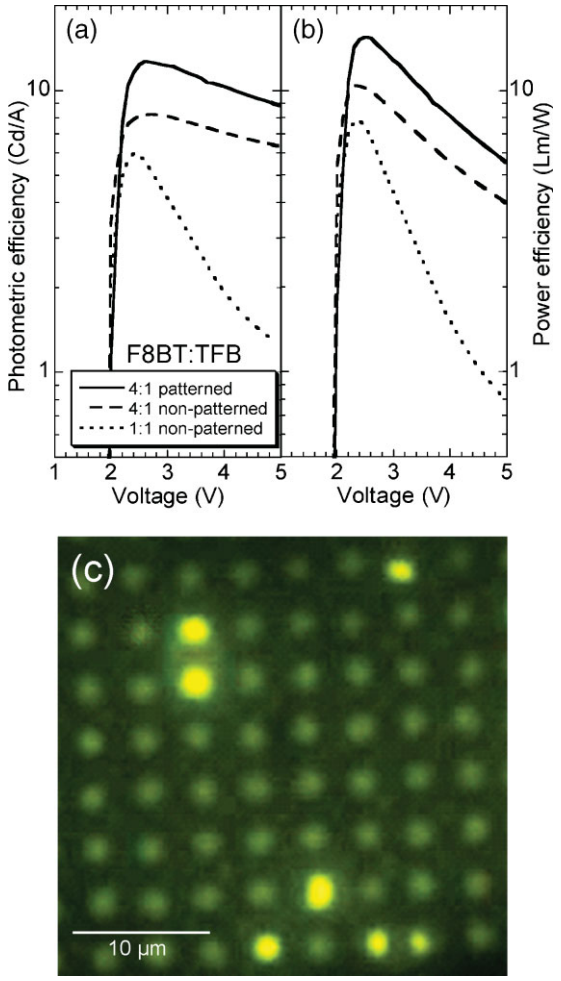

Figure 3. EL efficiency-voltage characteristics of LED fabricated with the patterned blend film expressed in a) $Cd\,A^{-1}$ and b) $Lm\,W^{-1}$. F8BT:TFB blend devices (4:1 and 1:1 by weight) prepared by spin-coating are included for comparison. c) EL image of the patterned blend device driven at 7 V, showing preferential yellow-green luminescence of F8BT from enclosed TFB-rich domains. Differences in brightness between the TFB-rich domains might be due to thickness variation across the blend film.

than PFO:F8BT due to better hole-injection/transport properties of TFB than PFO with the inclusion of triarylamine units along the polymer backbone that lowers the hole-injection barrier.

We observe that the reference F8BT:TFB (1:1 by weight) blend devices show high initial efficiencies just after turn-on ($6\,Cd\,A^{-1}$ and $8\,Lm\,W^{-1}$ at 2.4 V, EQE of ~1.9%), but decreases rapidly at high voltages ($1.3\,Cd\,A^{-1}$ and $0.8\,Lm\,W^{-1}$ at 4.9 V). Such device characteristics are closely related to the blend thin film morphology shown in Figure 2b. Phase separation in this blend film was studied elsewhere and the proposed cross section of the blend film is illustrated by the schematic drawing in Figure 5b.[12,15] While the continuous TFB wetting layer might assist hole injection/transport and act as an electron blocking layer at the anode interface, the discontinuous TFB capping layer might localize electron injection from the cathode, resulting in a high degree of spatial confinement of charge carriers. This then leads to high electron-hole capture efficiency at F8BT-TFB interfaces, which explains the observed high initial EL efficiencies in this blend device. However, the very rough blend film morphology with very thin lower-lying TFB-rich domains provides a pathway for holes to arrive at the cathode without undergoing radiation recombination, particularly at high voltages. Such imbalance of charge carriers causes an increase in leakage current and hence the observed rapid decay in EL efficiencies.[15]

In contrast, the reference F8BT:TFB devices with 4:1 blend composition show relatively slower decay in EL efficiencies at high voltages, taking away one of the drawbacks observed in the 1:1 blend devices. For example, the peak EL efficiency was $8\,Cd\,A^{-1}$ ($10\,Lm\,W^{-1}$, EQE of ~2.5%) at 2.4 V and the efficiency maintained at $6\,Cd\,A^{-1}$ ($4\,Lm\,W^{-1}$) at 5 V. We attribute such device characteristics to the smaller phase-separated structures and reduced roughness in its blend film shown in Figure 2c.

Relative to both reference blend devices, the patterned blend devices with self-organized 2D micrometer-scale structures exhibit even higher initial EL efficiency, while decaying again less than 1:1 blend devices at high voltages. The patterned blend film shows $13\,Cd\,A^{-1}$ ($15\,Lm\,W^{-1}$, EQE of ~4%) at 2.6 V and $9\,Cd\,A^{-1}$ ($6\,Lm\,W^{-1}$) at 5 V. We note that the observed improvement in LED performance for the patterned blend device is not likely to be caused by the additional oxygen-plasma treatment of the PEDOT:PSS layer required prior to patterning, as this step contributes to a slight decrease (~10%) in EL efficiencies for both the reference devices (not shown).

To investigate the underlying mechanisms responsible for the improved device performance, we analyzed the EL image of the patterned device, which is shown in Figure 3c (driven at 7 V). Strong yellow-green EL emission (from F8BT) appears as dots from the enclosed TFB (or TFB-rich) phases, while the continuous F8BT (or F8BT-rich) domain remains relatively dark at all voltages. This suggests that the phase-separated TFB lateral domains are not pure and contain significant proportion of both polymers. The EL emission observed in this patterned F8BT:TFB blend device is remarkably different from a normal blend device, where EL emission is predominantly produced at the interfaces between F8BT-rich and TFB-rich domains.[4] We attribute this to localized hole injection into the enclosed TFB-rich domains in the patterned film, which would imply the absence of a continuous TFB wetting layer typically formed in non-patterned F8BT:TFB blend films (Fig. 5b).[12] Such observation is intuitively reasonable; the fact that the phase-separated structures closely replicate the underlying 2D pattern demonstrates that substrate surface energy contrast (hydrophilic vs. hydrophobic) dominates over polymer surface energy contrast in determining the preferential wetting of the substrate by either of the two polymers.

This EL image clearly demonstrates the important role of controlled and localized charge injection into the active layer in determining the distribution of luminescence. We note that the

ADVANCED FUNCTIONAL MATERIALS

variation in the local electric field as a result of thickness differences between F8BT-rich and TFB-rich domains (~30 nm in ~300 nm thick film) is unlikely to the main cause for the observed EL only from the enclosed TFB-rich domains in the patterned device. This is because in a non-patterned 1:1 F8BT:TFB blend device, where the thickness variation across the phase separated domains is much higher (~40 nm in ~80 nm thick film) and thus the local electric field is much stronger, the lower-lying TFB-rich domains still remain dark at all voltages, while EL occurs only at the interfaces of different domains.[4]

Micro-Raman spectroscopy measurements were used to probe the chemical compositions of the phase-separated lateral domains in the patterned blend film.[12] The measurements were repeated after successive oxygen-plasma etching of the blend film, to investigate the presence of possible vertical segregation of the polymers within each of the two micrometer-scale lateral structures. Shown in Figure 4a is a Raman image of the patterned F8BT:TFB blend film based on Raman intensity contrast at 1546 cm^{-1}, which corresponds to the BT ring stretching mode in F8BT. The bright regions in the Raman image represent F8BT enrichment while the dark regions correspond to TFB enrichment. The Raman image of the unpatterned area (refer to the PL image in Fig. 1b) obtained in a similar way is shown in Figure 4b. These Raman images are qualitatively in agreement with the PL image (Fig. 1b), as both indicate that the enclosed domains are enriched with TFB while the continuous phases are F8BT-rich.

Figure 4c shows normalized Raman spectra of pristine F8BT and TFB thin films, along with those from different lateral domains in the patterned blend film, after background-correction against the underlying PEDOT:PSS layer. Both F8BT and TFB show strong Raman peak at 1609 cm^{-1} (fluorene ring stretch). Additionally, the Raman spectrum of TFB shows a partially resolved Raman peak at 1602 cm^{-1} (phenylene ring stretch), while F8BT shows a strong and distinct Raman peak at 1546 cm^{-1} (BT ring stretch). These unique Raman peaks of both polymers can be used as chemical signatures for the materials to quantitatively determine the compositions of the phase-separated domains, after calibrating the relative Raman scattering cross section for the materials. The relative Raman scattering cross section of the materials was obtained at 785 nm excitation using dilute blend solutions of known compositions, as previously described in the literature.[12]

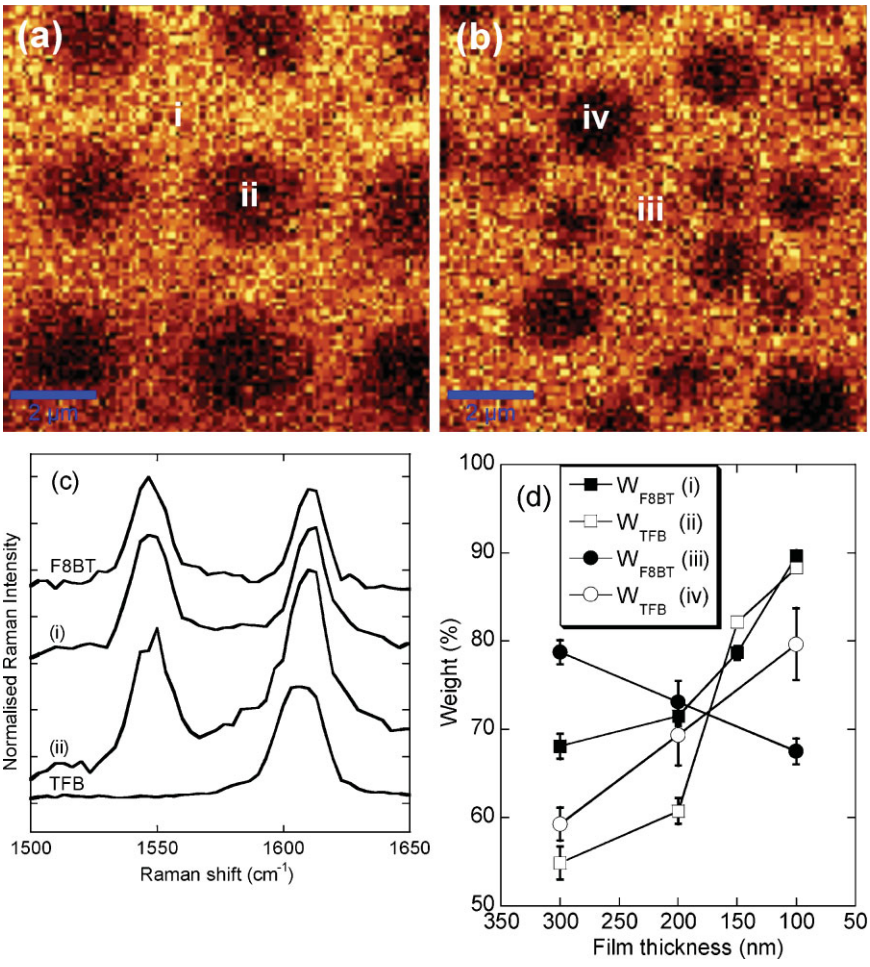

Figure 4. a) Raman image (10 μm × 10 μm) of the patterned F8BT:TFB blend film based on Raman intensity at 1546 cm^{-1} (BT ring stretch in F8BT). The bright regions correspond to F8BT-rich phases while the dark regions correspond to TFB-rich phases. b) The corresponding Raman image of the unpatterned area in the same blend film (refer to the top part of the PL image in Fig. 1b). c) Raman spectra taken in two different lateral domains of the patterned F8BT:TFB blend film, along with those of pristine F8BT and TFB thin films. d) Evolution of the chemical compositions of the two different domains in the ~300 nm-thick patterned F8BT:TFB blend film as it underwent successive oxygen plasma etching steps to reach a final thickness of ~100 nm. Similar analysis of the unpatterned area in the same blend film (shown in (b)) is included for comparison.

Figure 4d summarizes the evolution of the chemical compositions of the two different domains in the ~300 nm-thick patterned F8BT:TFB blend film as it underwent successive oxygen plasma etching steps to reach a final thickness of ~100 nm. Similar analysis of the unpatterned area in the same blend film (Fig. 4b) is included for comparison.

Prior to etching, we observe that both the phase-separated domains in the patterned F8BT:TFB blend film contain a significant proportion of both materials. For instance, the F8BT percentages of the continuous F8BT-rich phases and enclosed TFB-rich domains were 68% and 45% (by weight), respectively. This supports the observation of yellow-green F8BT emission from TFB-rich domains in

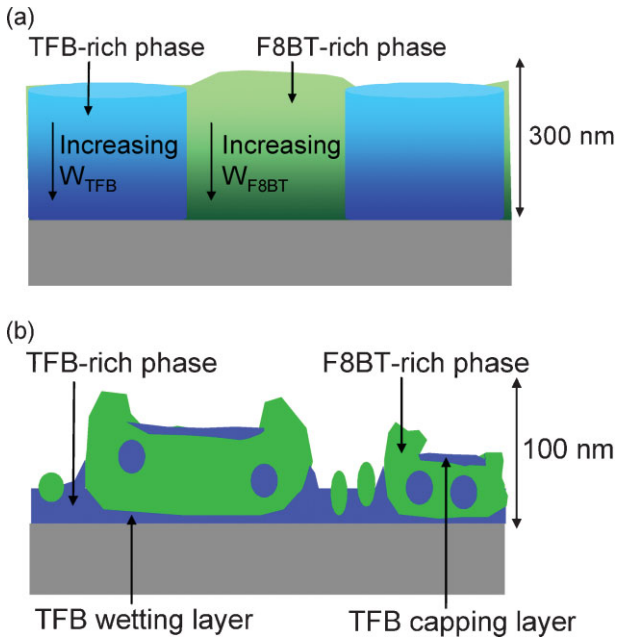

Figure 5. a) Schematic drawing summarizes the proposed cross section of the patterned F8BT:TFB blend film based on micro-Raman compositional analysis. Both domains show increased purity of the corresponding polymer nearer to the patterned substrate. b) Proposed cross section of a F8BT:TFB blend film spin-coated on non-patterned substrates, showing the presence of continuous TFB wetting layer and discontinuous TFB-capping layer, along with micrometer-scale lateral phase separation [12,15].

the EL image, due to the significant amount of F8BT materials present in these domains.

With successive etching of the patterned blend film, both domains gradually became purer with the respective materials. At the final film thickness of ~100 nm, both phases were almost completely depleted of the minority materials, showing ~90% enrichment in the dominating materials (TFB in the enclosed domains and F8BT in the continuous domains). This indicates that the presence of substrate surface energy contrast induced by the hydrophobic SAM of OTS exerts a stronger driving force for preferential lateral segregation of the two polymers, leading to a high degree of purity of polymers in both domains closer to the substrate. The effect of the surface pattern gradually diminishes, explaining the more disordered and mixed structures near the air-film interface.

In contrast to the patterned blend film, the unpatterned area of the blend film shows a different trend in the vertical phase segregation of the polymers, particularly in the F8BT-rich domains. As the blend film was gradually etched to ~100 nm, the F8BT-rich domains were gradually depleted of F8BT, with its relative composition decreasing from ~78% to ~68%. Referring to the schematic drawing in Figure 5b, this can be understood as the gradual exposure of the underlying continuous TFB wetting layer while the F8BT materials were being etched away.[9]

Based on the structural information obtained from the Raman analysis, we attempt to summarize the micrometer-scale lateral and nanometer-scale vertical phase segregation of the patterned F8BT:TFB blend film in the schematic drawing in Figure 5a. For both phase-separated lateral domains, there is a gradual change in the compositions across the blend film thickness, such that the film-substrate interface is highly enriched with either polymer according to their preference for substrate surface energy. Such characteristic lateral and vertical phase segregation of the polymers provides important insights into the EL processes in a working LED. In the absence of a continuous TFB wetting layer at the substrate interface, hole injection from PEDOT:PSS layer preferentially takes place at the enclosed TFB-rich domains, which represent a TFB/F8BT heterojunction structure with gradually-changing concentration, that is suitable for device operation. On the other hand, the continuous F8BT-rich domains represent a reversed heterojunction structure (F8BT closer to anode and TFB closer to cathode), which is unfavorable for charge carrier injection from both electrodes. This explains the observed well-defined and localized EL emission as dots from the enclosed domains, which subsequently leads to increased charge carrier confinement and recombination efficiency, and thus the observed increase in initial EL efficiency. Meanwhile, the slower decay observed in EL efficiency at high voltages is attributed to reduced surface roughness in the patterned blend film. With this understanding, in principle, one could engineer the lateral phase separation with a similar approach to increase the area density of the domain where EL takes place (in this case, the dots) to further enhance the luminance of the device.

In comparison, the schematic drawing in Figure 5b shows the typical phase separated structures in non-patterned F8BT:TFB blend films. Of particular importance is the formation of a continuous TFB wetting layer at the film-substrate interface. With the introduction of substrate surface energy contrast, the wetting of the substrate by either of the polymers, and subsequently the phase separated structures can be controlled.

We further investigated the possible effects on surface out-coupling of light emission in the presence of such periodic phase-separated structures in the patterned blend devices. Figure 6a shows normalized angular dependent EL measurement of the patterned F8BT:TFB blend device, in comparison with those of reference spin-coated blend devices (4:1 and 1:1 by weight) and F8BT-only devices. In the absence of any phase-separated structures in the active layer, such as F8BT-only devices, the EL emission is Lambertian as expected.[14] However, all the blend (including with/without patterning) devices show improved surface out-coupling of light emission in the forward direction, albeit to a different extent. Crucially, this suggests that the scattering of the waveguide mode out of the plane of the device is not unique to the patterned device, but is also present in all the other reference blend devices studied where the phase-separated structures are spatially random. This is despite the lack of ''ripple'' structures previously observed in patterned PFO:F8BT blend devices associated with waveguide out-coupling.[19] Hence, the improved performance of the patterned blend device (relative to the reference blend devices) must be attributed more to the

ADVANCED FUNCTIONAL MATERIALS

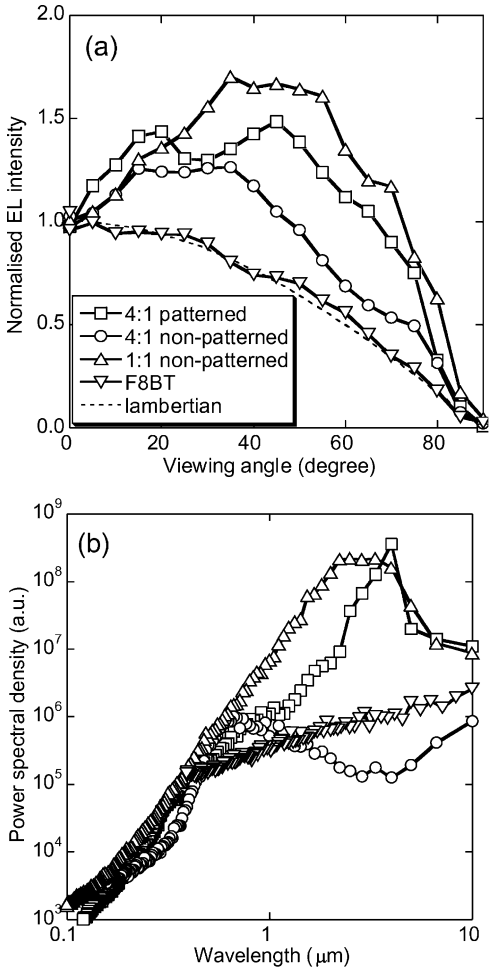

Figure 6. a) Angular dependent EL measurement of the patterned F8BT:TFB blend device, in comparison with that of spin-coated blend devices (4:1 and 1:1 by weight) and F8BT-only device. b) Power spectral density based on AFM images of the same set of blend and pristine films shows the distribution of periodicity in the phase-separated structures.

appropriate confinement of charge carriers within the phase-separated structures, as discussed earlier, than optical effects that harness waveguide mode trapped in polymer LEDs.

We performed Fourier transform analysis on the AFM images of the same set of films to analyze the distribution of periodicity in the blend film structures,[27] where the power spectra density is shown in Figure 6b. The patterned blend film shows a well-defined peak at ~4 μm, in agreement with the periodicity of the underlying 2D chemical pattern. On the other hand, normal F8BT:TFB 1:1 blend film, for instance, shows a broader distribution of periodicity of the phase-separated structures, which is again expected from its AFM image (Fig. 2b).

Comparing Figure 6a and b, qualitatively, we observe positive correlation between the extent of surface out-coupling of light emission and the distribution of periodicity in the phase-separated structures. This can be understood by considering the amount of light scattering in the presence of phase-separated structures with different optical properties (such as refractive indices). It appears that having a well-defined periodicity in the phase-separated structures does not particularly assist the out-coupling of waveguide mode. For instance, the F8BT:TFB 1:1 blend film shows the broadest distribution of periodicity in its phase-separated structures while having the largest surface out-coupling of light in the forward direction. The precise relationship between the periodicity of phase-separated structures and the out-coupling of waveguide mode might require more detailed device modelling, but this observation certainly suggests the possibility of harnessing waveguide mode trapped in LEDs by appropriately controlling the periodicity of the phase-separated structures in the active layer.

Note that the overall device efficiency is determined by not only such optical effects (surface out-coupling of light emission) but also the electronic processes (such as localized charge injection and recombination) within the active layer. Hence, among the blend devices studied here, the normal F8BT:TFB 1:1 blend has the largest surface out-coupling of light while showing the lowest EL efficiency. It is therefore essential to consider both the electronic processes and optical effects for further device optimization.

3. Conclusion

We have shown the control of the phase separation of F8BT:TFB blend films by introducing a chemical pattern on the substrate for surface energy modification, which has subsequently led to improved LED performance. A periodic contrast of the substrate surface energy was created by μCP of OTS on the oxygen-plasma treated PEDOT:PSS surface. With appropriate choice of polymer molecular weight and blend ratio, the phase-separated structures in the blend film closely replicate the underlying 2D OTS pattern since TFB preferentially migrate away from regions of higher surface energy. Micro-Raman analysis revealed nanometer-scale vertical segregation of the polymers within both lateral domains, with regions closer to the substrate being substantially pure with each of the two polymers. This indicates the absence of a continuous TFB wetting layer typically formed in blend films spin-coated on non-patterned surfaces, and has important implications on device performance. It also implies the formation of periodic TFB/F8BT (and reversed) heterojunction structures which favor (and suppress) charge carrier injection from both electrodes in the TFB-rich (F8BT-rich) domains. As a result, charge carrier injection is confined in the well-defined enclosed TFB-rich domains, leading to high EL efficiency. The overall reduction in the patterned blend film roughness as compared to reference spin-coated blend (1:1 by weight) leads to slower decay in EL efficiency at high voltages. The amount of surface out-coupling of light in the forward direction observed in blend devices is also found to be

positively correlated to the distribution of periodicity of the phase-separated structures in the active layer.

4. Experimental

Polymer solutions were prepared by dissolving each polymer in *p*-xylene to produce a concentration of 16 mg mL^{-1} for F8BT ($M_n = 62$ kg mol^{-1}) and 17 mg mL^{-1} for TFB ($M_n = 66$ kg mol^{-1}). For the blends, F8BT and TFB solutions were mixed at a ratio of either 4:1 or 1:1 (by weight). Polymer films of ~80–100 nm-thick were then spin-coated from these solutions onto pre-cleaned quartz substrates.

Surface-directed phase separation of blend films using the micro-contact printing technique was performed on a layer of spin-coated PEDOT:PSS.[24–26] After thermal annealing treatment of the PEDOT:PSS layer, it was briefly oxygen-plasma treated at 250 W for 30 s to create hydroxyl groups for silanization. A poly(dimethylsiloxane) PDMS stamp, featuring 2D pattern of 2-μm-wide dots with 4 μm periodicity, was used to periodically deposit a SAM of covalently-bound and hydrophobic OTS onto the PEDOT:PSS layer. A polymer blend of F8BT:TFB (4:1 weight ratio) was then spin-coated onto this patterned surface for 1 s and left to dry slowly for at least 1 h under saturated solvent atmosphere conditions.

LEDs were fabricated by using ITO as anode, F8BT:TFB blend film as the active layer, and Ca/Al as cathode. A ~60-nm-thick PEDOT:PSS layer was first spin-coated onto oxygen-plasma treated ITO-coated glass substrate and then baked at 200 °C for 1 h under N_2 flow, prior to the deposition of the polymer blend film. Finally, Ca (~20 nm) with an Al (~100 nm) protecting layer was thermally evaporated at a base pressure of ~10^{-6} mbar. The EL spectra of encapsulated LEDs were measured as a function of viewing angle, in planes perpendicular to the device surface, using a silica fiber bundle mounted on a home-built goniometer, which was fed into a calibrated Oriel spectrometer.

For Micro-Raman spectroscopy measurements, samples (blend films deposited on quartz substrates) were excited in a 180° backscattering geometry by a 785 nm laser diode (~1 mW) focussed through a 100x objective in a WITec confocal Raman microscope. The Rayleigh-scattered light was eliminated by an edge filter such that only the Raman-scattered light dispersed by a grating was collected by a Peltier-cooled deep-depletion CCD detector. Spectra accumulation of 0.3 s was used for 10 μm × 10 μm Raman scans, allowing quick qualitative identification of the phase separated domains. For quantitative determination of the materials composition in different domains of the blend film, spectra accumulation of 50 s was used. The Raman spectra were corrected for dark noise from the detector, fluorescent background from the polymers and Raman scattering from the underlying PEDOT:PSS layer. For vertical phase segregation analysis, the patterned F8BT:TFB blend film underwent successive oxygen plasma etching steps of 250 W for 5 minutes, with an average etching rate of ~10 nm min^{-1}.

Received: February 28, 2008
Revised: April 25, 2008
Published online: September 9, 2008

[1] R. H. Friend, R. W. Gymer, A. B. Holmes, J. H. Burroughes, R. N. Marks, C. Taliani, D. D. C. Bradley, D. A. Dos Santos, J.-L. Brédas, M. Lögdlund, W. R. Salaneck, *Nature* **1999**, *397*, 121.
[2] P. K. H. Ho, J. S. Kim, J. H. Burroughes, H. Becker, S. F. Li, T. M. Brown, F. Cacialli, R. H. Friend, *Nature* **2000**, *404*, 481.
[3] J. J. M. Halls, C. A. Walsh, N. C. Greenham, E. A. Marseglia, R. H. Friend, S. C. Moratti, A. B. Holmes, *Nature* **1995**, *376*, 498.
[4] A. C. Morteani, A. S. Dhoot, J. S. Kim, C. Silva, N. C. Greenham, C. Murphy, E. Moons, S. Ciná, J. H. Burroughes, R. H. Friend, *Adv. Mater.* **2003**, *15*, 1708.
[5] J. J. M. Halls, J. Cornil, D. A. dos Santos, R. Silbey, D.-H. Hwang, A. B. Holmes, J.-L. Brédas, R. H. Friend, *Phys. Rev. B* **1999**, *60*, 5721.
[6] H. M. P. Wong, P. Wang, A. Abrusci, M. Svensson, M. R. Andersson, N. C. Greenham, *J. Phys. Chem. C.* **2007**, *111*, 5244.
[7] E. Moons, *J. Phys. Condens. Matter* **2002**, *14*, 12235.
[8] J. J. M. Halls, A. C. Arias, J. D. MacKenzie, W. Wu, M. Inbasekaran, E. P. Woo, R. H. Friend, *Adv. Mater.* **2000**, *12*, 498.
[9] Y. Xia, R. H. Friend, *Adv. Mater.* **2006**, *18*, 1371.
[10] J. S. Kim, P. K. H. Ho, C. Murphy, N. Baynes, R. H. Friend, *Adv. Mater.* **2002**, *14*, 206.
[11] S. Walheim, M. Böltau, J. Mlynek, G. Krausch, U. Steiner, *Macromolecules* **1997**, *30*, 4995.
[12] J. S. Kim, P. K. H. Ho, C. E. Murphy, R. H. Friend, *Macromolecules* **2004**, *37*, 2861.
[13] J. Chappell, D. G. Lidzey, P. C. Jukes, A. M. Higgins, R. L. Thompson, S. O'Connor, I. Grizzi, R. Fletcher, J. O'Brien, M. Geoghegan, R. A. L. Jones, *Nat. Mater.* **2003**, *2*, 616.
[14] J. S. Kim, P. K. H. Ho, N. C. Greenham, R. H. Friend, *J. Appl. Phys.* **2000**, *88*, 1073.
[15] K. H. Yim, W. J. Doherty, W. R. Salaneck, R. H. Friend, J. S. Kim, unpublished.
[16] N. Corcoran, A. C. Arias, J. S. Kim, J. D. Mackenzie, R. H. Friend, *Appl. Phys. Lett.* **2003**, *82*, 299.
[17] A. C. Arias, J. D. Mackenzie, R. Stevenson, J. J. M. Hall, M. Inbasekaran, E. P. Woo, D. Richards, R. H. Friend, *Macromolecules* **2001**, *34*, 6005.
[18] G. Fichet, N. Corcoran, P. K. H. Ho, A. C. Arias, J. D. Mackenzie, W. T. S. Huck, R. H. Friend, *Adv. Mater.* **2004**, *16*, 1908.
[19] N. Corcoran, P. K. H. Ho, A. C. Arias, Mackenzie, R. H. Friend, G. Fichet, W. T. S. Huck, *Appl. Phys. Lett.* **2004**, *85*, 2965.
[20] M. Böltau, S. Walheim, J. Mlynek, G. Krausch, U. Steiner, *Nature* **1998**, *391*, 877.
[21] G. Krausch, E. J. Kramer, M. H. Rafailovich, J. Sokolov, *Appl. Phys. Lett.* **1994**, *64*, 2655.
[22] Y. Xia, G. M. Whitesides, *Angew. Chem. Int. Ed.* **1998**, *37*, 551.
[23] A. Kumar, G. M. Whitesides, *Appl. Phys. Lett.* **1993**, *63*, 2002.
[24] X. Li, R. Xing, Y. Zhang, Y. Han, L. An, *Polymer* **2004**, *45*, 1637.
[25] J. Raczkowska, P. Cyganik, A. Budkowski, A. Bernasik, J. Rysz, I. Raptis, P. Czuba, K. Kowalski, *Macromolecules* **2005**, *38*, 8486.
[26] P. Andrew, W. T. S. Huck, *Soft Matter* **2007**, *3*, 230.
[27] W. Ma, C. Yang, A. J. Heeger, *Adv. Mater.* **2007**, *19*, 1387.